

# Dependence of Two-proton Radioactivity on Nuclear Pairing Models

Tomohiro Oishi,<sup>1,2,3,\*</sup> Markus Kortelainen,<sup>2,1</sup> and Alessandro Pastore<sup>4</sup>

<sup>1</sup>*Helsinki Institute of Physics, P.O. Box 64, FI-00014 University of Helsinki, Finland*

<sup>2</sup>*Department of Physics, P.O. Box 35 (YFL), University of Jyväskylä, FI-40014 Jyväskylä, Finland*

<sup>3</sup>*Research Center for Electron Photon Science, Tohoku University, 1-2-1 Mikamine, Sendai 982-0826, Japan*

<sup>4</sup>*Department of Physics, University of York, Heslington, York YO10 5DD, United Kingdom*

The sensitivity of two-proton emitting decays to the nuclear pairing correlation is discussed within a time-dependent three-body model. We focus on the  ${}^6\text{Be}$  nucleus assuming  $\alpha + p + p$  configuration, and its decay process is described as a time-evolution of the three-body resonance state. A noticeable model-dependence of two-proton decay width is found by utilizing schematic density-dependent contact (SDDC) and the finite-range Minnesota pairing models. The model-dependence with the SDDC pairing interaction can be understood by monitoring the time-dependent density distribution, which reflects (i) density dependence of pairing correlation inside the core, and (ii)  $p - p$  scattering properties in vacuum. Our result suggests that two-proton decay width can be a suitable reference quantity to sophisticate the nuclear pairing model beyond the nucleon driplines.

PACS numbers: 21.10.Tg, 21.45.-v, 23.50.+z, 27.20.+n

## I. INTRODUCTION

Description of nuclear pairing correlation has been a major subject in recent nuclear physics. For instance, in self-consistent meanfield (SCMF) description of atomic nuclei, there have been various approaches in order to take the nuclear pairing correlation into account [1–6]. These approaches based on the SCMF or the nuclear density functional theory (DFT) have provided considerable agreements with the measured binding energy as well as its odd-even staggering for bound nuclei. Even with these efforts, however, the complete character of the nuclear pairing correlation has not been revealed. For example, whether the phenomenological pairing interaction should have the volume or surface type of density dependence is still an open question [7–10]. At present, one can find several candidates for the sophisticated nuclear pairing model [7–12]. In order to validate these models, one may need reference observables to fit not only for bound nuclei. Also, it should be emphasized that the pairing correlation near and beyond the neutron and proton driplines could play a fundamental role to determine the limit of existence on the nuclear chart [13, 14].

Recently, it has been expected that the two-proton ( $2p$ ) radioactivity may provide novel information on the nuclear pairing correlation. In the true  $2p$  emission [15–17], a pair of protons is emitted simultaneously from the parent nucleus, whereas the single-proton emission is forbidden or strongly suppressed due to the pairing correlation energy. The proton-proton pairing plays an essential role to determine the observables, especially the released energy (Q-value) as well as the  $2p$ -decay width or lifetime [18, 19]. The released Q-value can be related with the proton-proton pairing strength in bound nuclei. On the other hand, the  $2p$ -decay width has no correspon-

dence in bound systems, whose lifetime is trivially infinite. Thus,  $2p$  decays may provide another lodestar with new experimental input to optimize and validate the pairing models. Thanks to the experimental developments, there has been a considerable accumulation of data for the  $2p$ -emitting nuclei [20–22]. On the other side, however, theoretical studies have not been sufficient to clarify the relation between the  $2p$  radioactivity and the pairing correlation [23, 24]. Because  $2p$  emission is a typical many-body problem, its elucidation could also provide an universal knowledge on the multi-particle quantum phenomena in various domains. Those include, *e.g.* the quantum entanglement [25], BCS-BEC crossover [26, 27], and Efimov physics [28–30].

In this article, we discuss how the theoretical characters of pairing models are reflected on  $2p$ -decay properties, connected to a specific interest in sophisticating those models. For this purpose, we employ the time-dependent three-body model [19], whose simplicity enables us to phenomenologically understand the pairing model-dependence of  $2p$  radioactivity. We focus on the  $2p$  emission from the ground state of the  ${}^6\text{Be}$  nucleus, assuming the configuration of two valence protons and a rigid  $\alpha$  core.

Formalism of our model is given in Sec. II. In Sec. III, we present numerical calculations and discussions. Finally Sec. IV is devoted to summarize the article.

## II. THREE-BODY MODEL

Details of the time-dependent three-body calculations are present in Ref.[19]. In this article, we employ the same method with some expansions. The  $2p$  decay from  ${}^6\text{Be}$  is described as a time-evolution of the two protons in the spherical mean-field generated by the  $\alpha$  core. The three-body Hamiltonian is given as [27, 31–34],

$$H_{3b} = h_1 + h_2 + \frac{\mathbf{p}_1 \cdot \mathbf{p}_2}{A_c m} + v_{p-p}(\mathbf{r}_1, \mathbf{r}_2), \quad (1)$$

\* Present e-address: toishi@pd.infn.it

where  $h_i = \mathbf{p}_i^2/2\mu + V_{c-p}(r_i)$  ( $i = 1, 2$ ) is the single particle (s.p.) Hamiltonian between the core and the  $i$ -th proton.  $\mu \equiv mA_c/(A_c + 1)$  is the reduced s.p. mass with  $A_c = 4$ .

The core-proton potential is given as  $V_{c-p}(r) = V_{WS}(r) + V_{Coul}(r)$ . Woods-Saxon potential is expressed as

$$V_{WS}(r) = V_0 f(r) + U_{ls}(\mathbf{l} \cdot \mathbf{s}) \frac{1}{r} \frac{df(r)}{dr}, \quad (2)$$

with a function,  $f(r) = 1/[1 + e^{(r-R_0)/a_0}]$ , which can be related to the density-distribution of the core.  $V_{Coul}$  describes Coulomb potential. For  $f(r)$  and  $V_{Coul}(r)$ , we employ the same parameters as in Ref.[19], in order to reproduce the resonance energy and width in the  $(p_{3/2})$ -channel of  $\alpha - p$  scattering,  $\epsilon_r = 1.96$  MeV and  $\Gamma_r \simeq 1.5$  MeV, respectively [35]. Note that this resonance is attributable to the centrifugal potential barrier [19].

The  $p - p$  pairing potential is introduced as  $v_{p-p} = v_{p-p}^{(N)} + e^2/|\mathbf{r}_1 - \mathbf{r}_2|$ . Here, we employ a schematic density-dependent contact (SDDC) potential,

$$v_{p-p}^{(N)}(\mathbf{r}_1, \mathbf{r}_2) = w(|(\mathbf{r}_1 + \mathbf{r}_2)/2|) \delta(\mathbf{r}_1 - \mathbf{r}_2), \quad (3)$$

$$w(r) = w_0 [1 - \eta f(r)],$$

for nuclear pairing interaction. Here two protons have an contact pairing correlation, whose density-dependence is schematically approximated as the  $\eta f(r)$  term. Notice also that  $w(r \rightarrow \infty) = w_0$ . For intrinsic two-nucleon structures, including the dinucleon correlation, similar three-body model calculations with SDDC pairing models have been utilized [27, 31–34], with a consistency between other theoretical results [36–39].

With the contact interaction, it is generally known that one should introduce the energy cutoff,  $E_{cut}$ , in order to avoid the ultra-violet divergence [40]. In present case, the bare strength,  $w_0$ , can be determined so as to reproduce the empirical scattering length of nucleons in vacuum,  $a_0 = -18.5$  fm, consistently to the energy-cutoff [31, 32]. That is,

$$w_0 = \frac{4\pi^2 \hbar^2 a_0}{m(\pi - 2a_0 k_{cut})}, \quad (4)$$

with  $k_{cut} = \sqrt{mE_{cut}}/\hbar$ . The cutoff energy is set as  $E_{cut} = 40$  MeV similarly in Ref.[19], yielding  $w_0 = -767.4$  MeV·fm<sup>3</sup>.

Total expectation value of  $H_{3b}$ , which is conserved during the time-evolution, corresponds to the released Q-value of the three-body decay. That is,

$$Q_{2p} = \langle \Psi(t) | H_{3b} | \Psi(t) \rangle, \quad (5)$$

$$= \langle h_1 + h_2 \rangle_{(t)} + \Delta_{pair}(t),$$

$$\Delta_{pair}(t) = \left\langle \Psi(t) \left| \frac{\mathbf{p}_1 \cdot \mathbf{p}_2}{A_c m} + v_{p-p}(\mathbf{r}_1, \mathbf{r}_2) \right| \Psi(t) \right\rangle, \quad (6)$$

where  $\Delta_{pair}$  is the pairing correlation energy (PCE). In order to reproduce the empirical Q-value,  $1371 \pm 5$  keV

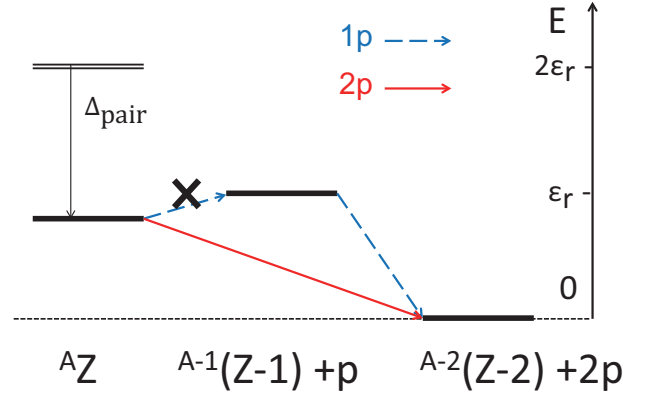


FIG. 1. Schematic figure of level scheme, in which the correlated  $2p$  emission becomes dominant.

[35], we also employ a density-dependence parameter,  $\eta = 1.04$  in Eq.(3), corresponding to the surface type of the SDDC pairing interaction. Indeed, it schematically describes the surface type of the density-dependent pairing interaction in meanfield calculations [7–9]. Note also that PCE approximately corresponds to the pairing gap when the system is bound.

We assume the  $0^+$  configuration for two protons and the  $\alpha$  core, consistently to the total spin-parity which is also  $0^+$  for the ground state of  ${}^6\text{Be}$ . Thus, the eigen-states of the three-body Hamiltonian,  $H_{3b} |E_N\rangle = E_N |E_N\rangle$ , can be expanded on  $0^+$  basis:

$$|E_N\rangle = \sum_M U_{NM} |\Phi_M\rangle, \quad (7)$$

$$\Phi_M(\mathbf{r}_1, \mathbf{r}_2) = \hat{\mathcal{A}}[\phi_{n_a l j m}(\mathbf{r}_1) \otimes \phi_{n_b l j (-m)}(\mathbf{r}_2)]^{0^+}, \quad (8)$$

with the simplified notation,  $M = (n_a, n_b, l, j)$ .  $\hat{\mathcal{A}}$  is the anti-symmetrization operator. The expansion coefficients,  $U_{NM}$ , are determined by diagonalizing the Hamiltonian matrix for  $H_{3b}$ . Each s.p. state satisfies  $h_i \phi_{n l j m}(\mathbf{r}_i) = \epsilon_{n l j} \phi_{n l j m}(\mathbf{r}_i)$ , with the radial quantum number  $n$ , the orbital angular momentum  $l$ , the spin-coupled angular momentum  $j$  and the magnetic quantum number  $m$ . We employ the s.p. states up to the  $(h_{11/2})$ -channel. In order to take into account the Pauli principle, we exclude the first  $s_{1/2}$  state, which is occupied by the protons in the core nucleus. The continuum s.p. states ( $\epsilon_{n l j} > 0$ ) of  $V_{c-p}$  are discretized in the radial box of  $R_{box} = 80$  fm. Thus, continuum eigenstates of  $H_{3b}$  are also discretized. As we present in Sec.III C, this radial box is sufficiently large to provide a good convergence in terms of the decay width.

It is worthwhile to mention that, if one neglects PCE,  $2p$ -resonance state locates at  $Q_{2p} = \langle h_1 + h_2 \rangle = 2\epsilon_r$ , where  $\epsilon_r$  is the  $\alpha - p$  resonance energy. In this case, where  $2p$ -wave function keeps the pure  $(p_{3/2})^2$  configuration, it was confirmed that the decay process is well described as a sequential  $2p$  emission [19]. Taking PCE into account, the resonance energy is decreased mainly due to

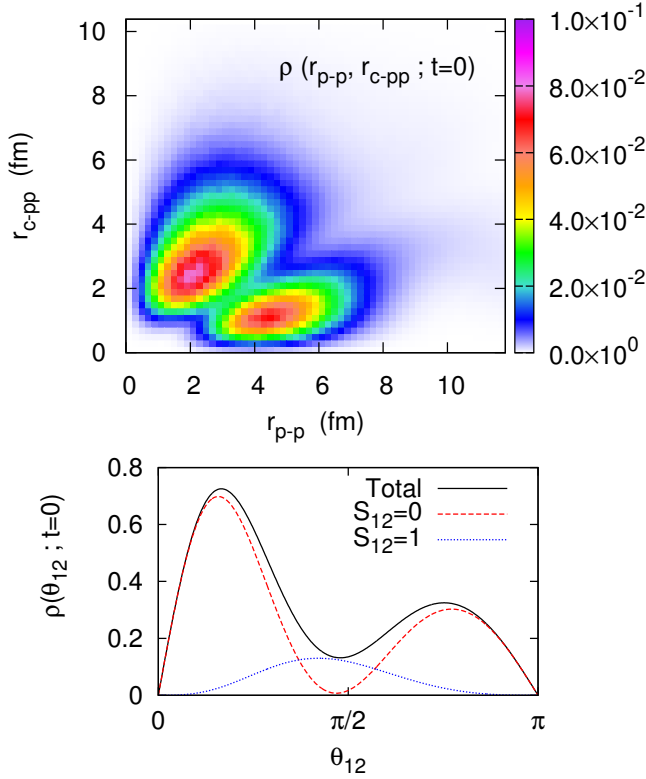


FIG. 2. The density-distribution for the initial  $2p$  state obtained with the surface SDDC pairing interaction. (i) Top panel: the distribution as a function of  $r_{p-p}$  and  $r_{c-pp}$ . (ii) Bottom panel: the angular distribution as a function of the opening angle,  $\theta_{12}$ , between two protons. This is obtained by integrating  $\rho(r_1, r_2, \theta_{12})$  for the radial coordinates,  $r_1$  and  $r_2$ . The spin-singlet and spin-triplet components are also plotted.

the attractive pairing interaction. Figure 1 schematically describes this situation. In Ref.[19], the finite-range and density-independent Minnesota potential was employed to describe the pairing force [41], and then the strongly correlated  $2p$  emission was suggested.<sup>1</sup> To occur the spatial correlation in this process, mixture of other configurations from  $(p_{3/2})^2$  plays an essential role [27, 33].

### III. NUMERICAL CALCULATION

#### A. Initial State

In order to fix the initial state for time-evolution, we employ the same confining potential,  $V_{c-p}^{\text{conf}}(r)$ , as in Ref.[19]. This confining potential method has provided good approximations for quantum resonance phenomena

<sup>1</sup> We found a typo in Table I of Ref.[19]: “ $S = 0$  (1)” should be corrected as “ $S = 1$  (0)”.

[23, 42–44], together with an intuitive way to understand their dynamics. The initial state solved within the confining Hamiltonian can be expanded on the eigen-basis of the original Hamiltonian:  $|\Psi(0)\rangle = \sum_N F_N(0) |E_N\rangle$ . Thus, the time-evolution is represented as

$$|\Psi(t)\rangle \equiv \exp\left[-it\frac{H_{3b}}{\hbar}\right] |\Psi(0)\rangle = \sum_N F_N(t) |E_N\rangle, \quad (9)$$

where  $F_N(t) = e^{-itE_N/\hbar} F_N(0)$ . It is worthwhile to note that the time-invariant discrete energy spectrum can be given as

$$d(E_N) = |F_N(0)|^2 = |F_N(t)|^2. \quad (10)$$

If one takes the continuous energy limit,  $d(E)$  resembles the Breit-Wigner (BW) spectrum, which characterizes the quantum resonance properties of concerning radioactive process [45].

In Fig. 2, we plotted the normalized density distribution for the initial state. That is,

$$\rho(t; r_1, r_2, \theta_{12}) = 8\pi^2 r_1^2 r_2^2 \sin \theta_{12} |\Psi(t; r_1, r_2, \theta_{12})|^2, \quad (11)$$

at  $ct = 0$  fm. For convenience,  $\rho$  is translated to a function of the relative distance between the two protons,  $r_{p-p} = (r_1^2 + r_2^2 - 2r_1 r_2 \cos \theta_{12})^{1/2}$ , and that between the core and the center of mass of two protons,  $r_{c-pp} = (r_1^2 + r_2^2 + 2r_1 r_2 \cos \theta_{12})^{1/2}/2$ . From Fig. 2, we find the similar result in Ref.[19], where a finite-range pairing interaction was used instead: the higher peak at  $r_{p-p} \simeq 2.0$  fm and  $r_{c-pp} \simeq 2.5$  fm, as well as at  $\theta_{12} \simeq \pi/6$ , indicates a strong localization of two protons. Notice also that this localization is attributable to the spin-singlet configuration, suggesting a diproton correlation [34].

#### B. Time-evolution

In Fig. 3, we plotted the time-development of  $2p$  state, in terms of the probability-density distribution. It is well described that the confined two protons at  $ct = 0$  are released during the time-development. The probability-density outside the core-proton barrier gradually increases, indicating an evacuation of two protons. In order to monitor their decay dynamics more preciously, it is helpful to focus on the projected decay state [25]. That is,

$$|\Psi_d(t)\rangle \equiv |\Psi(t)\rangle - \beta(t) \cdot |\Psi(0)\rangle, \quad (12)$$

with  $\beta(t) = \langle \Psi(0) | \Psi(t) \rangle$ . Because the initial state is well confined, this projected decay state mainly represents the outgoing components released from around the core. In Fig. 4, we plot the density distribution of the projected decay state normalized at each point of time. That is,

$$\rho_d(t; r_1, r_2, \theta_{12}) = \frac{8\pi^2 r_1^2 r_2^2 \sin \theta_{12} |\Psi_d(t; r_1, r_2, \theta_{12})|^2}{N_d(t)}, \quad (13)$$

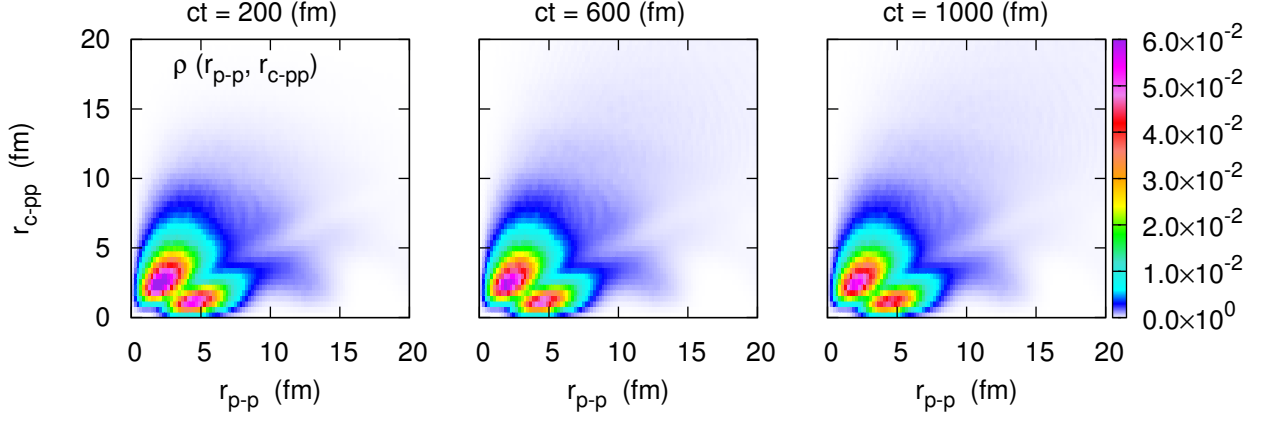


FIG. 3. Time-dependent  $2p$ -density distribution plotted as a function of  $r_{p-p}$  and  $r_{c-pp}$ . The surface SDDC pairing interaction is employed.

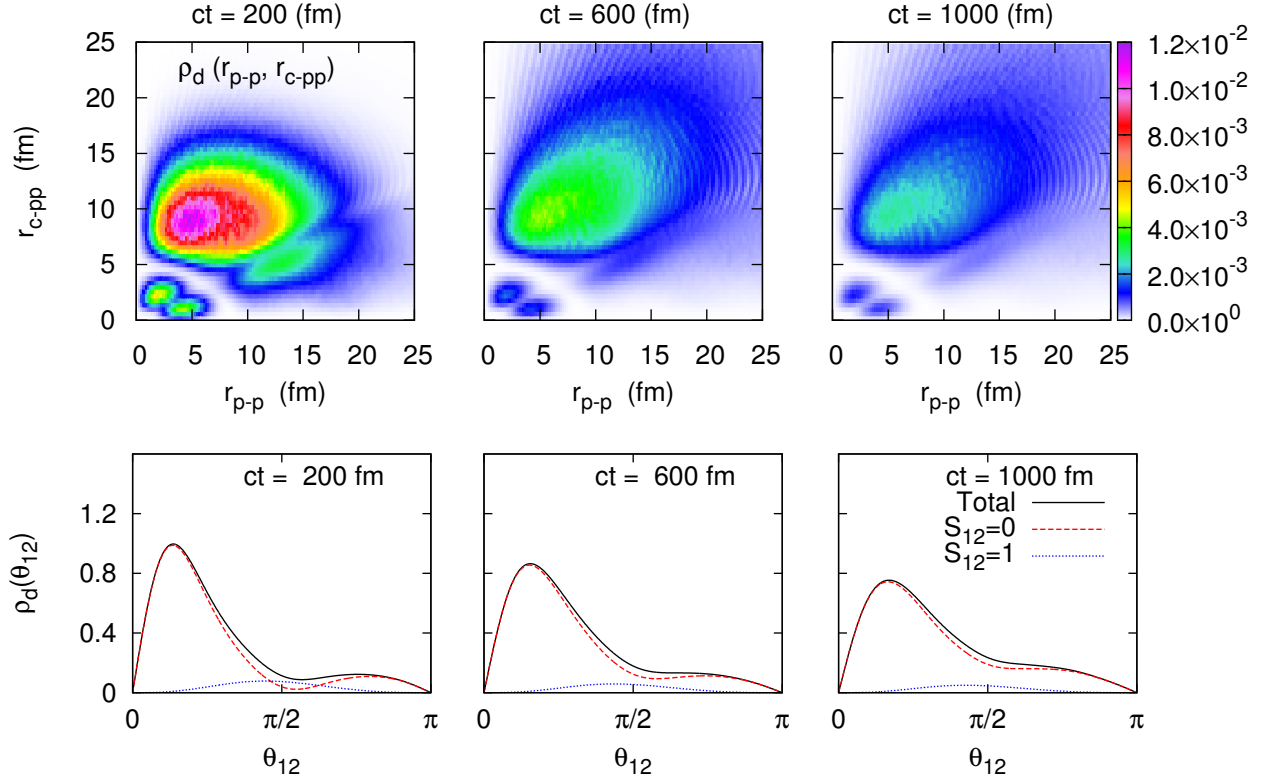


FIG. 4. Time-dependent  $2p$ -density distribution of the decay state,  $\rho_d(t)$ , given by Eq. (13). The surface SDDC pairing interaction is employed. These are plotted in the same manner as in Fig. 2.

where  $N_d(t) = \langle \Psi_d(t) | \Psi_d(t) \rangle = 1 - |\beta(t)|^2$  is the decay probability. In Fig. 4, the strongly correlated  $2p$ -emission is suggested with our surface SDDC pairing model. The diproton correlation, which can be detected as a peak at  $r_{p-p} \simeq 5$  fm and  $r_{c-pp} \simeq 10$  fm, as well as at  $\theta_{12} \simeq \pi/6$ , is dominant during the time-evolution. Notice also that the sequential  $2p$  emission, which is graphically

indicated as a ridge along the  $r_{c-pp} \simeq r_{p-p}/2$  line [19], is strongly suppressed. This dynamical behavior of protons is similar to that suggested from the finite-range Minnesota pairing model [19].

TABLE I. Parameters for SDDC pairing interactions used in this article. Resultant Q-values of the  $2p$  emission of  ${}^6\text{Be}$  and the corresponding total, spin-singlet and spin-triplet decay widths at  $ct = 1000$  fm are also present. Results obtained with the softened, finite-range Minnesota pairing model are fetched from Ref.[19].

	$w_0$ (MeV·fm <sup>3</sup> )	$\eta$	$Q_{2p}$ (keV)	$\Gamma$ (keV)	$\Gamma_{S=0}$ (keV)	$\Gamma_{S=1}$ (keV)
SDDC (Surface)	-767.4	1.04	1370.7	34.7	33.4	1.3
SDDC (Mixed)	-623.3	0.50	1370.9	24.0	22.7	1.3
SDDC (Volume)	-525.5	0.00	1370.6	19.7	18.3	1.4
SDDC (Emitter)	-1036.8	1.80	1367.6	90.3	89.5	0.8
Minnesota [19]			1370.7	88.2	87.1	1.1
Experiment [35]			$1371 \pm 5$	$92 \pm 6$	—	—

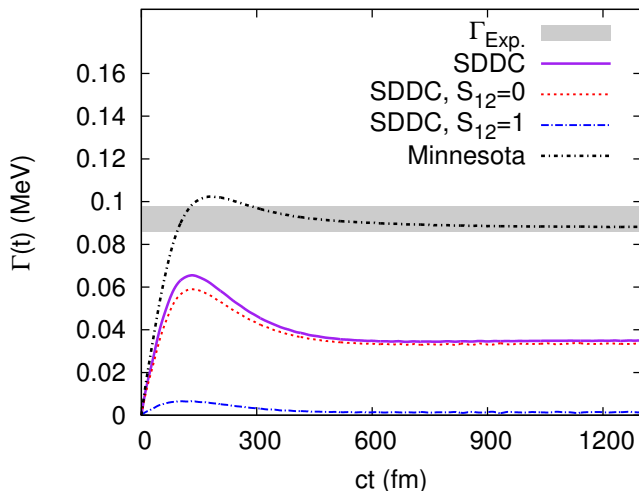


FIG. 5. The  $2p$ -decay width of  ${}^6\text{Be}$  obtained from the surface SDDC pairing interaction. The spin-singlet ( $S_{12} = 0$ ) and spin-triplet ( $S_{12} = 1$ ) widths are both plotted. The total width obtained with the finite-range Minnesota pairing is taken from Ref. [19]. Experimental result,  $\Gamma = 92 \pm 6$  keV, is indicated by the shaded area [35].

### C. Decay Width

We next investigate the decay width, which is one of the directly measurable quantities of the  $2p$  emission. From the decay probability,  $N_d(t)$ , the  $2p$ -decay width is calculated as

$$\Gamma(t) = -\hbar \frac{d}{dt} \ln[1 - N_d(t)] = \frac{\hbar}{1 - N_d(t)} \frac{d}{dt} N_d(t). \quad (14)$$

It is worthwhile to note that, if the time-evolution follows the exponential decay rule, which is a fundamental property of radioactive processes, the decay probability is given as  $N_d(t) = 1 - \exp(-t\Gamma_c/\hbar)$ . Here  $\Gamma_c$  is the constant decay width. In this case,  $\Gamma(t)$  becomes identical to  $\Gamma_c$ , which determines the mean lifetime of this system,  $\tau = \hbar/\Gamma_c$ .

In Fig. 5, we plotted the actually calculated decay width as a function of time. With the SDDC pairing interaction, we finally obtain the convergence of result after a sufficient time-evolution. From Krylov-Fock theorem [45, 46], this coincides with that the energy distribution,  $d(E_N)$ , well approximates the BW spectrum, and thus reproduces the exponential decay rule.  $\Gamma(t)$  at  $ct = 1000$  fm is 34.7 keV, as tabulated in Table I. In Fig. 5, for a comparison, we fetch the result with the finite-range Minnesota pairing force [19].

From these results, we find that the SDDC pairing interaction underestimates the experimental  $2p$ -decay width, whereas the finite-range Minnesota pairing showed a good agreement with it. Remember that, as present in Table I, both pairing models are adjusted so as to reproduce the same Q-value, corresponding to an equivalent condition on the PCE. Also, the core-proton potential and the cutoff parameters are common in both cases. Thus, the difference in  $2p$ -decay width should be purely attributed to the pairing properties. In Fig. 5, the partial decay widths for the spin-singlet and spin-triplet channels are also plotted [19]:  $\Gamma(t) = \Gamma_{S=0}(t) + \Gamma_{S=1}(t)$ . One finds again the dominance of the spin-singlet configuration in  $2p$  emission consistently to the density distribution in Fig. 4. The exact values of  $\Gamma_{S=0,1}(t)$  at  $ct = 1000$  fm are also summarized in Table I. With the SDDC pairing, the spin-singlet  $2p$ -decay width is remarkably small compared with the Minnesota pairing case, whereas the spin-triplet width shows the similar values in both cases.

The smaller width in the SDDC pairing case might be attributable to the numerical sensitivity. For radioactive processes governed by the quantum tunneling effect, even a small difference in Q-value can yield a large change of the resultant decay width. In order to check this sensitivity, we run the same calculations but changing the absolute strength of the pairing force. That is,  $v_{p-p}^{(N)} \rightarrow f \cdot v_{p-p}^{(N)}$  with  $f = 0.990, 0.995, 1.005$ , and  $1.010$ , whereas  $f = 1$  exactly corresponds to the empirical Q-value. Because the pairing interaction is attractive, a reduction of it ( $f < 1$ ) yields the enhanced Q-value, meaning that the resonance energy is shifted to the higher

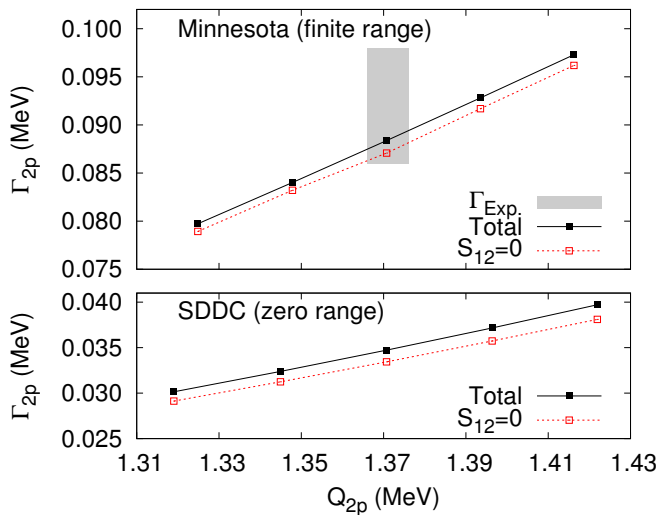


FIG. 6. The  $2p$ -decay width as a function of the emission  $Q$ -value,  $Q_{2p}$ , obtained with the Minnesota and the surface SDDC pairing interactions. The 5 points of results are plotted for each case:  $f \cdot v_{p-p}^{(N)}$  with  $f = 1.010, 1.005, 1.000, 0.995$ , and  $0.990$ , ordered as from left to right on each panel. Experimental result,  $Q_{2p} = 1371 \pm 5$  keV and  $\Gamma_{2p} = 92 \pm 6$  keV, is indicated by the shaded area [35].

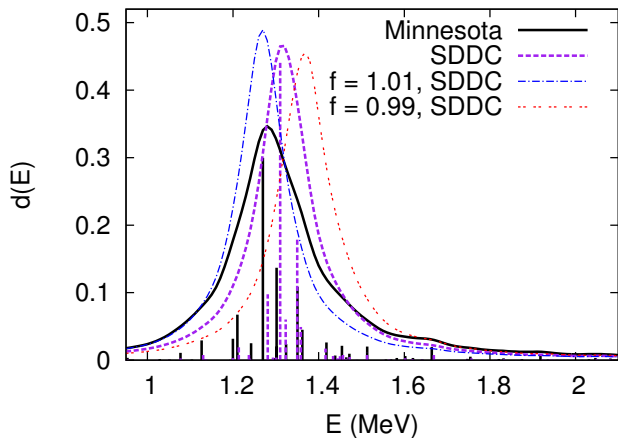


FIG. 7. Time-invariant discrete energy distributions,  $d(E_N)$ , obtained with the Minnesota and the surface SDDC pairing interactions. Continuous distributions, which are plotted in the arbitrary scale, are obtained by smearing  $d(E_N)$  with a Cauchy-Lorentz function, whose full width at the half maximum is  $\Gamma = 0.1$  MeV. The same continuous plots but for the enhanced (reduced) surface SDDC pairing with  $f = 1.010$  ( $0.990$ ) are also displayed.

region.

The  $Q_{2p}$ - $\Gamma_{2p}$  relation obtained with the different pairing strengths is present in Fig. 6. Obviously, the enhanced (reduced)  $Q$ -value leads to the increase (decrease) of the decay width. This can be kinetically understood as that the enhanced  $Q$ -value increases the penetrability

of the potential barrier and then yields the larger width, which is equivalent to the shorter lifetime. Similarly in Table I, the spin-singlet width is universally dominant, whereas the spin triplet width, indicated by the gap of the total and the spin-singlet widths, shows the similar values in both cases. In our calculations throughout several  $Q_{2p}$  values, the SDDC pairing commonly yields the smaller width than the Minnesota pairing. Consequently, the difference in  $\Gamma_{2p}$  is not attributable to the  $Q$ -value sensitivity, but concluding the pairing model-dependence. Note also that, with the SDDC pairing, we could not reproduce the empirical  $Q_{2p}$  and  $\Gamma_{2p}$  simultaneously, even within the experimental uncertainties.

In Fig. 7, the discrete energy spectra,  $d(E_N)$ , and their continuous distributions smeared by a Cauchy-Lorentz function are plotted. We see that the spectrum width obtained with the SDDC pairing model is not sensitive to the peak position, and it is narrower than that with the Minnesota pairing model. This result coincides with the  $\Gamma_{2p}$  values shown in Fig. 6.

#### D. Density-dependence

In the remaining of this section, we investigate what in the SDDC pairing model essentially controls the  $2p$ -decay width. In SCMF or DFT calculations, so-called volume and mixed types of density-dependent pairing interaction have been employed as often as the surface type [7–9]. These characters of density-dependence can be approximated by  $\eta = 0, 1/2$ , and  $1$  in Eq.(3) for volume, mixed, and surface types, respectively. In order to investigate the role of density-dependence, we perform the similar calculations by changing  $\eta$ , in addition to the original, surface SDDC case ( $\eta = 1.04$ ).

For  $\eta = 0.0$  and  $0.5$ , we change the pairing strength,  $w_0$ , so as to reproduce the same reference  $Q$ -value. Those parameters are summarized in Table I. Notice that changing  $w_0$  corresponds to the different value of vacuum-scattering length.

In Fig. 8, we plot the decay widths obtained with different SDDC parameterizations. It is found that the volume SDDC pairing yields the smallest  $\Gamma_{2p}$  value, whereas the mixed pairing reproduces the medium result between the surface and volume cases. Considering the experimental reference quantities, the surface SDDC pairing somehow provides the best improvement among three cases. Here we also employ an *emitter* SDDC potential with  $\eta = 1.8$  to help our discussion. Its parameters are also tabulated in Table I. With this model, we indeed obtain a good agreement with experiment: as shown in Fig. 8 and Table I, the emitter SDDC pairing can reproduce the experimental  $Q$ -value and decay width simultaneously. Consequently, fixing the same reference  $Q$ -value,  $2p$ -decay width is connected to the density-dependence parameter,  $\eta$ .

In the top panel of Fig. 9, we plot the contact pairing strength,  $w(r)$  in Eq.(3), for several SDDC parameter-



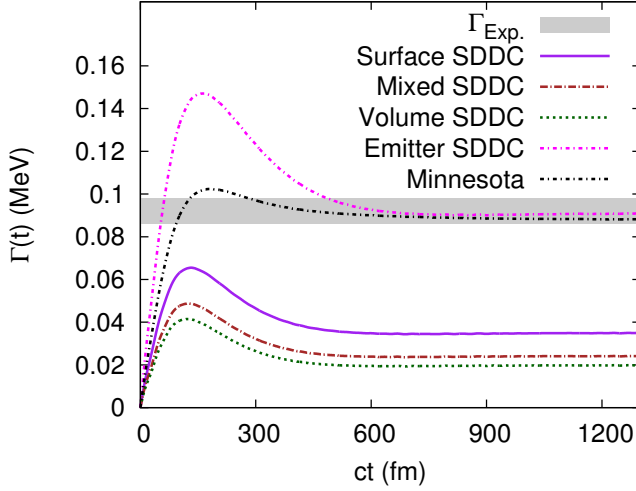


FIG. 8.  $2p$ -decay widths of  ${}^6\text{Be}$  obtained from the various pairing models.

izations. It is worthwhile to emphasize that, with the emitter SDDC model, the pairing interaction is repulsive and thus the pairing correlation becomes unstable deeply inside the core. Also, due to the deeper  $w_0$  value, two protons in vacuum earn a larger PCE than that with other SDDC models.

The sensitivity of  $2p$ -decay width is now understood from a synergy of pairing correlations in two regions. For this purpose, in Fig. 9, we present the one-proton probability-density distribution of the initial and time-developed states. That is,

$$\rho_1(t; r) = 8\pi^2 \int_0^{R_{\text{box}}} dr_2 r_2^2 \int_{-1}^1 d(\cos \theta_{12}) \times |\Psi(t; r, r_2, \theta_{12})|^2. \quad (15)$$

Because our  $2p$ -basis functions are anti-symmetrized,  $|\Psi(\mathbf{r}_1, \mathbf{r}_2)|^2$  is symmetric for the exchange of  $\mathbf{r}_1$  and  $\mathbf{r}_2$ . Thus,  $\rho_1(t; r)$  represents the mean radial distribution of  $2p$  probability.

From Fig. 9, in the surface and emitter SDDC cases, the probability density shows a dispersive shape. This is a product of (i) weak or repulsive pairing inside the core, as well as (ii) strong  $p-p$  interaction in vacuum. The first effect drives out the two-proton wave function tunneling the potential barrier, whereas the second favors a large probability density outside the core. This mechanism then yields a loose stability with shorter mean lifetime. On the other hand, in the volume SDDC case, two-proton density hardly diverges with the isotropically attractive pairing interaction. Note that this mechanism commonly exists during the time-evolution, because the total Hamiltonian itself is time-independent.

With the present simple SDDC interaction,  $\eta$  and  $w_0$  are not independent parameters to fit: when one is fixed, another should be determined consistently to  $Q_{2p}$ . Thus,

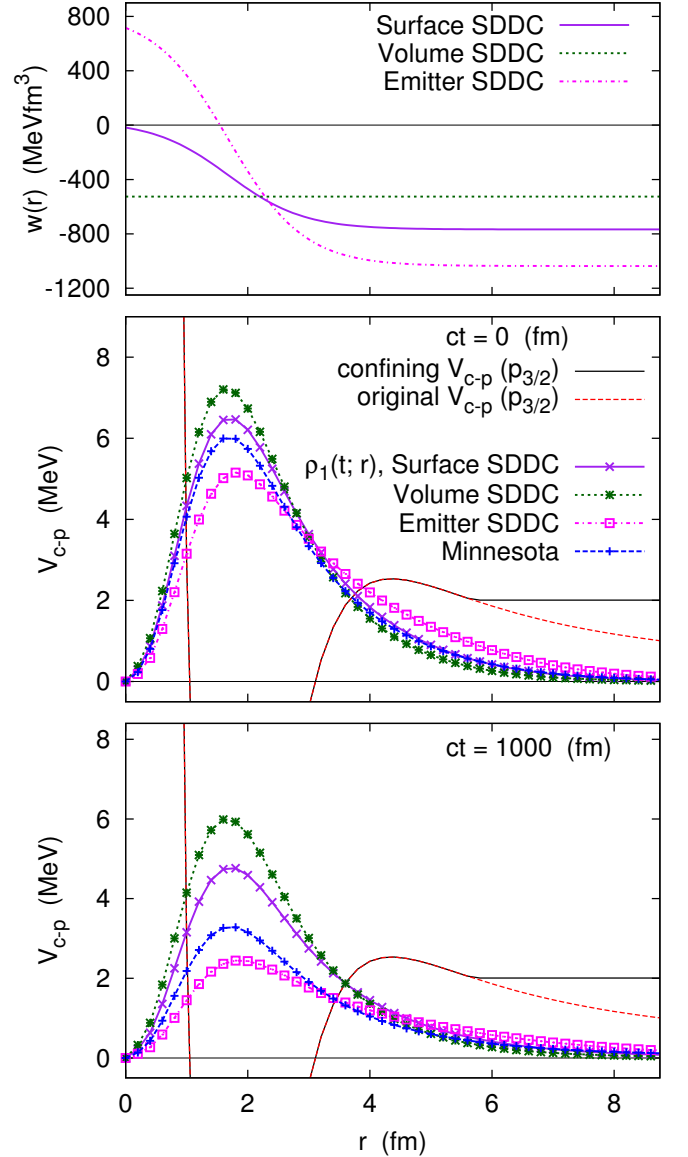


FIG. 9. (i) Top panel: The radial strength,  $w(r)$ , for the SDDC pairing potential,  $v_{p-p}^{(N)}(\mathbf{r}_1, \mathbf{r}_2) = w(r_1) \cdot \delta(\mathbf{r}_1 - \mathbf{r}_2)$ . Note that  $w(r \rightarrow \infty) = w_0$ . (ii) Middle and bottom panels: The one-proton density-distributions at  $ct = 0$  and  $1000$  fm, respectively. These distributions are plotted in the arbitrary scale. Confining and original potentials in the  $(p_{3/2})$  channel of  $\alpha-p$  subsystem are also plotted.

model-dependence of  $\Gamma_{2p}$  contains two effects from (i) the density-dependent pairing inside the core, and (ii)  $p-p$  scattering properties in vacuum [20]. At this moment, however, separation of these effects is not trivial. One possible approach is to employ a non-trivial parameterization of the density-dependence. This approach could also help to resolve *tri-lemma* problem detailed in the next subsection.

Lastly, we have confirmed that our conclusions do not change even if we employ a smaller value of  $E_{\text{cut}}$ .

We recalculated the decay width with  $E_{\text{cut}} = 32$  MeV, with SDDC pairing strength renormalized to reproduce  $Q_{2p} = 1.37$  MeV. The obtained results reproduced the same width  $\Gamma(t)$ , as with the higher cutoff.

### E. Tri-lemma Problem of Two-proton Emitter

We mention an unnegligible problem raised from our results. Namely, there is a *tri-lemma* of  $Q_{2p}$ ,  $\Gamma_{2p}$ , and the two-nucleon scattering length in vacuum,  $a_0$ .

In three-body model calculations for bound systems, all the two-body interactions are prepared to reproduce the partial two-body subsystems. Additionally, in order to reproduce the three-body binding energy, one often takes the dynamical effect into account. Density-dependent pairing model is a phenomenological procedure for this purpose. For bound systems, this method works if the three-body picture is adequate.

The situation changes for unbound  ${}^6\text{Be}$ . With SDDC pairings combined with the well-adjusted core-proton potential for  $\alpha - p$ , (i) in the case of  $\eta = 1.04$  (surface),  $\Gamma_{2p}$  is not reproduced, where we keep  $a_0$  and  $Q_{2p}$  consistently to experiments. (ii) With  $\eta = 1.8$  (emitter), we reproduce the experimental  $Q_{2p}$  and  $\Gamma_{2p}$ , whereas the pairing strength,  $w_0$ , is inevitably modified inconsistently to the experimental scattering length. This is the tri-lemma of  $a_0$ ,  $Q_{2p}$ , and  $\Gamma_{2p}$ . Note that this problem could be also found in Ref.[19], where the softened Minnesota pairing reproduces only  $Q_{2p}$  and  $\Gamma_{2p}$ .

In this work, certain SDDC parameterization to resolve this problem has not been found. One possible solution is to employ a non-trivial parameterization of the density-dependence,  $w(r)$ , in the pairing force. The new  $w(r)$  should differ from our surface SDDC function inside the core, whereas they should have the same  $w_0$  value in vacuum. Another possible solution is phenomenological three-body force [17, 50]. It may provide both the three-body dynamical effect and the asymptotic two-body properties consistently to experiments. Because these considerable solutions inevitably harm the simplicity of the present model, we leave these developments as a subject of future study.

Although this tri-lemma remains, our conclusion about the pairing model-dependence in  $2p$ -decay width is not changed. In order to improve theoretical pairing models, which can be connected to the effective pairing force in DFT calculations, modern experimental data of  $2p$ -emitters may provide adequate reference quantities.

### F. Range-sensitivity Problem

Before closing our discussion, we mention another sensitivity to the range of pairing force. The  $p-p$  Minnesota

potential used in previous calculations was given as

$$v_{p-p}^{(N)} = V_{\text{Min}} = v_r e^{-d^2/2q^2} + v_s e^{-d^2/2\kappa_s^2 q^2} \cdot \hat{P}_{S=0} + v_t e^{-d^2/2\kappa_t^2 q^2} \cdot \hat{P}_{S=1}, \quad (16)$$

where  $d \equiv |\mathbf{r}_1 - \mathbf{r}_2|$ ,  $v_r = 156$  MeV,  $v_s = -91.85$  MeV,  $v_t = -178$  MeV,  $q = 0.5799$  fm,  $\kappa_s = 1.788$ , and  $\kappa_t = 1.525$ .  $\hat{P}_{S=0(1)}$  is the projection to the spin-singlet (triplet) channel. Remember that  $v_r$  was softened from the original value,  $v_r = 200$  MeV [41], in order to reproduce the reference Q-value. Here the first term describes a soft repulsive core. Decomposing  $d^2 = x^2 + y^2 + z^2$ , this term reads as

$$v_r e^{-d^2/2q^2} = w_r \frac{e^{-x^2/2q^2} \cdot e^{-y^2/2q^2} \cdot e^{-z^2/2q^2}}{(2\pi)^{3/2} q^3}, \quad (17)$$

where  $w_r = v_r (2\pi)^{3/2} q^3 = 479.1$  MeV·fm<sup>3</sup>, and similarly as expected for the following attraction terms. Utilizing a well known formula,

$$\lim_{q \rightarrow 0} \frac{e^{-x^2/2\kappa^2 q^2}}{q\sqrt{2\pi}} = \delta(x/\kappa) = |\kappa| \delta(x), \quad (18)$$

then at zero-range limit, we obtain

$$\lim_{q \rightarrow 0} V_{\text{Min}}(\mathbf{r}_1, \mathbf{r}_2) = w_0 \delta(\mathbf{r}_1 - \mathbf{r}_2), \quad (19)$$

where  $w_0 = w_r + \kappa_s^3 w_s = -1133.4$  MeV·fm<sup>3</sup>. Notice also that, for two-proton basis in  $0^+$  configuration, matrix elements of the spin-triplet contact potential become zero automatically from the angular-momentum algebra [47]. Indeed, this zero-range form is identical to the volume SDDC pairing given in Table I, but with the deeper bare strength.

Employing the volume SDDC pairing given in Eq. (19), however, we confirmed that the  $\alpha + p + p$  three-body system fictionally becomes bound with  $Q_{2p} \simeq -1.3$  MeV, where the decay width is trivially zero. In order to reproduce the experimental Q-value,  $Q_{2p} = 1.37$  MeV, we needed to use the shallower bare strength as in Table I. As a result, we obtained  $\Gamma_{2p} = 88.2$  and  $19.7$  keV with the finite-range and zero-range Minnesota potentials, respectively. This shows a sensitivity of  $2p$ -decay width to the interaction range.

To reinforce our conclusion, we repeat the same calculation but with the shorter range,  $q/\sqrt{2} \simeq 0.41$  fm in Eq.(16). In this case, we also need to employ the enhancement factor,  $f = 2.047$ , to reproduce the reference Q-value:  $v_{p-p}^{(N)} = f \cdot V_{\text{Min}}(q/\sqrt{2})$ . Resultant  $2p$ -decay widths are displayed in Fig.10. As expected, the short-range Minnesota yields the medium value of the decay width between the original and zero-range Minnesota cases.

Notice that, because Minnesota forces are density-independent, this range-sensitivity should be attributed



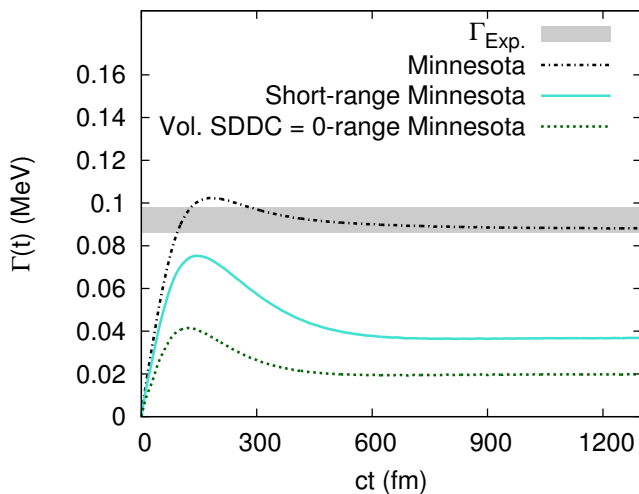


FIG. 10. Time-dependent  $2p$ -decay width of  ${}^6\text{Be}$  obtained with several Minnesota-pairing forces.

only to the vacuum scattering properties. Here we simply emphasize that the finite range could be an alternative option instead of the density-dependence, in order to reproduce the concerning  $2p$ -decay width and  $Q$ -value simultaneously.

#### IV. SUMMARY

We have discussed the dependence of  $2p$  radioactivity on nuclear pairing models within the time-dependent three-body model calculations. Comparing the zero-range SDDC and the finite-range Minnesota pairing forces, the  $2p$  dynamics is interpreted as the correlated  $2p$  emission similarly in both cases. Evaluating the absolute decay probabilities, we found that the two-proton decay width is remarkably sensitive to the pairing models, even with the equivalent condition on the emitted  $Q$ -value.

Within the SDDC pairing model, the  $2p$ -decay width significantly reflects the synergy of pairing correlations inside and outside the core. It controls the penetrability of  $2p$  density, confined in the core-proton potential barrier at the initial state reproducing the reference  $Q$ -value. The surface or emitter SDDC pairing provided the looser stability and thus the larger decay width.

Because our three-body Hamiltonian itself is not time-dependent nor self-consistent, it is not completely clear whether the similar density-dependence effect can be reflected on the SCMF or DFT calculations. Thus, it is suggestive to expand our procedure to these frameworks [48, 49], which enables us to perform the systematic investigation along the  $2p$ -drip line. The work toward this direction could be helpful to sophisticate the theoretical pairing models, utilizing the  $2p$ -decay data as the reference quantities. An experimental survey widely for the  $2p$ -emitter candidates could be profitable for this purpose [14].

With the simple SDDC pairing force, there remains a tri-lemma of  $Q_{2p}$ ,  $\Gamma_{2p}$ , and the two-nucleon scattering length in vacuum,  $a_0$ . In order to reproduce the whole two-body and three-body properties consistently to experiments, further model development is necessary.

We also found another kind of sensitivity to the range of pairing force. Considering the experimental  $Q$ -value, with the finite-range Minnesota potential, we finely reproduced the experimental  $2p$ -decay width [19]. On the other side, at the zero-range limit of that potential, theoretical  $2p$ -decay width is significantly narrow. Because the density-dependence is absent in these cases, there should be another logic to explain the different width. For this clarification, a further systematic analysis with respect of the interaction range may be helpful. Even it demands computational efforts, the work toward this direction is in progress now. Also, it might help to resolve the tri-lemma problem of  $2p$ -decay.

Comparison with other kind of experimental data, *e.g.* momentum distributions in Refs. [17, 51], is an important topic for future work. For this purpose, however, the present model space should be expanded sufficiently to reliably handle the long-range Coulomb effects. Although the computational cost is highly increased, it may provides another procedure to validate effective pairing models.

#### ACKNOWLEDGMENTS

T. Oishi sincerely thank Kouichi Hagino and Hiroyuki Sagawa for fruitful discussions. This work was supported by Academy of Finland and University of Jyväskylä within the FIDIPRO programme. We acknowledge the CSC-IT Center for Science Ltd., Finland, for the allocation of computational resources.

- 
- [1] D. Brink and R. Broglia, *Nuclear Superfluidity: Pairing in Finite Systems*, Cambridge Monographs on Particle Physics, Nuclear Physics and Cosmology (Cambridge University Press, Cambridge, UK, 2005).
  - [2] R. A. Broglia and V. Zelevinsky, eds., *Fifty Years of Nuclear BCS: Pairing in Finite Systems* (World Scientific, Singapore, 2013).

- [3] D. J. Dean and M. Hjorth-Jensen, *Rev. Mod. Phys.* **75**, 607 (2003).
- [4] M. Bender, P.-H. Heenen, and P.-G. Reinhard, *Rev. Mod. Phys.* **75**, 121 (2003).
- [5] J. Dobaczewski, W. Nazarewicz, T. R. Werner, J. F. Berger, C. R. Chinn, and J. Dechargé, *Phys. Rev. C* **53**, 2809 (1996).

- [6] T. Lesinski, T. Duguet, K. Bennaceur, and J. Meyer, The European Physical Journal A **40**, 121 (2009), and in private communications.
- [7] N. Sandulescu, P. Schuck, and X. Viñas, Phys. Rev. C **71**, 054303 (2005).
- [8] A. Pastore, F. Barranco, R. A. Broglia, and E. Vigezzi, Phys. Rev. C **78**, 024315 (2008).
- [9] A. Pastore, J. Margueron, P. Schuck, and X. Viñas, Phys. Rev. C **88**, 034314 (2013).
- [10] M. Grasso, Phys. Rev. C **87**, 064308 (2013).
- [11] S. A. Changizi and C. Qi, Phys. Rev. C **91**, 024305 (2015).
- [12] N. Pillet, N. Sandulescu, P. Schuck, and J.-F. Berger, Phys. Rev. C **81**, 034307 (2010).
- [13] J. Erler, N. Birge, M. Kortelainen, W. Nazarewicz, E. Olsen, A. M. Perhac, and S. Mario, Nature **486**, 509 (2012).
- [14] E. Olsen, M. Pfützner, N. Birge, M. Brown, W. Nazarewicz, and A. Perhac, Phys. Rev. Lett. **110**, 222501 (2013).
- [15] V. I. Goldansky, Nucl. Phys. **19**, 482 (1960).
- [16] V. I. Goldansky, Nucl. Phys. **27**, 648 (1961).
- [17] L. Grigorenko, T. Wiser, K. Miernik, R. Charity, M. Pfützner, A. Banu, C. Bingham, M. wiok, I. Darby, W. Dominik, J. Elson, T. Ginter, R. Grzywacz, Z. Janas, M. Karny, A. Korgul, S. Liddick, K. Mercurio, M. Rajabali, K. Rykaczewski, R. Shane, L. Sobotka, A. Stolz, L. Trache, R. Tribble, A. Wuosmaa, and M. Zhukov, Physics Letters B **677**, 30 (2009).
- [18] D. S. Delion, R. J. Liotta, and R. Wyss, Phys. Rev. C **87**, 034328 (2013).
- [19] T. Oishi, K. Hagino, and H. Sagawa, Phys. Rev. C **90**, 034303 (2014).
- [20] L. V. Grigorenko, Physics of Particles and Nuclei **40**, 674 (2009).
- [21] B. Blank and M. Płoszajczak, Reports on Progress in Physics **71**, 046301 (2008).
- [22] M. Pfützner, M. Karny, L. V. Grigorenko, and K. Riisager, Rev. Mod. Phys. **84**, 567 (2012).
- [23] T. Maruyama, T. Oishi, K. Hagino, and H. Sagawa, Phys. Rev. C **86**, 044301 (2012).
- [24] K. Hagino and H. Sagawa, Phys. Rev. C **89**, 014331 (2014).
- [25] C. Bertulani, M. Hussein, and G. Verde, Physics Letters B **666**, 86 (2008).
- [26] J. Margueron, H. Sagawa, and K. Hagino, Phys. Rev. C **76**, 064316 (2007).
- [27] K. Hagino, H. Sagawa, J. Carbonell, and P. Schuck, Phys. Rev. Lett. **99**, 022506 (2007).
- [28] V. Efimov, Physics Letters B **33**, 563 (1970).
- [29] P. F. Bedaque, H.-W. Hammer, and U. van Kolck, Phys. Rev. Lett. **82**, 463 (1999).
- [30] E. Hiyama and M. Kamimura, Phys. Rev. A **90**, 052514 (2014).
- [31] G. Bertsch and H. Esbensen, Annals of Physics **209**, 327 (1991).
- [32] H. Esbensen, G. F. Bertsch, and K. Hencken, Phys. Rev. C **56**, 3054 (1997).
- [33] K. Hagino and H. Sagawa, Phys. Rev. C **72**, 044321 (2005).
- [34] T. Oishi, K. Hagino, and H. Sagawa, Phys. Rev. C **82**, 024315 (2010), with erratum.
- [35] F. Ajzenberg-Selove, Nuclear Physics A **490**, 1 (1988).
- [36] M. Matsuo, K. Mizuyama, and Y. Serizawa, Phys. Rev. C **71**, 064326 (2005).
- [37] M. Matsuo, H. Shimoyama, and Y. Ootaki, Physica Scripta **T150**, 014024 (2012).
- [38] K. Hagino and H. Sagawa, Phys. Rev. C **75**, 021301 (2007).
- [39] Y. Kikuchi, K. Katō, T. Myo, M. Takashina, and K. Ikeda, Phys. Rev. C **81**, 044308 (2010).
- [40] A. Bulgac and Y. Yu, Phys. Rev. Lett. **88**, 042504 (2002).
- [41] D. Thompson, M. Lemere, and Y. Tang, Nuclear Physics A **286**, 53 (1977).
- [42] S. A. Gurvitz and G. Kalbermann, Phys. Rev. Lett. **59**, 262 (1987).
- [43] S. A. Gurvitz, Phys. Rev. A **38**, 1747 (1988).
- [44] S. A. Gurvitz, P. B. Semmes, W. Nazarewicz, and T. Vertse, Phys. Rev. A **69**, 042705 (2004).
- [45] V. I. Kukulin, V. M. Krasnopolsky, and J. Horáček, *Theory of Resonances: Principles and Applications*, Reidel Texts in the Mathematical Sciences, Vol. 3 (Springer-Verlag, Berlin and Heidelberg, Germany, 1989).
- [46] N. S. Krylov and V. A. Fock, Zh. Éksp. Teor. Fiz. **17**, 93 (1947).
- [47] Y. Tanimura, K. Hagino, and H. Sagawa, Phys. Rev. C **86**, 044331 (2012).
- [48] G. Scamps and D. Lacroix, Phys. Rev. C **87**, 014605 (2013).
- [49] S. Ebata, T. Nakatsukasa, and T. Inakura, Phys. Rev. C **90**, 024303 (2014).
- [50] T. Myo, K. Katō, S. Aoyama, and K. Ikeda, Phys. Rev. C **63**, 054313 (2001).
- [51] L. V. Grigorenko, T. D. Wiser, K. Mercurio, R. J. Charity, R. Shane, L. G. Sobotka, J. M. Elson, A. H. Wuosmaa, A. Banu, M. McCleskey, L. Trache, R. E. Tribble, and M. V. Zhukov, Phys. Rev. C **80**, 034602 (2009).